JACS
JOURNAL OF THE AMERICAN CHEMICAL SOCIETY

Article

pubs.acs.org/JACS

Kinetic Mechanism of Translocation and dNTP Binding in Individual DNA Polymerase Complexes

Kate R. Lieberman,*[,†] Joseph M. Dahl,[†] Ai H. Mai,[†] Ashley Cox,[†] Mark Akeson,[†] and Hongyun Wang*[,‡]

[†]Department of Biomolecular Engineering and [‡]Department of Applied Mathematics and Statistics, University of California, Santa Cruz, Baskin School of Engineering, 1156 High Street, MS: SOE2, Santa Cruz, California 95064, United States

Supporting Information

ABSTRACT: Complexes formed between phi29 DNA polymerase (DNAP) and DNA fluctuate discretely between the pre-translocation and post-translocation states on the millisecond time scale. The translocation fluctuations can be observed in ionic current traces when individual complexes are captured atop the α-hemolysin nanopore in an electric field. The presence of complementary 2′-deoxynucleoside triphosphate (dNTP) shifts the equilibrium across the translocation step toward the post-translocation state. Here we have determined quantitatively the kinetic relationship between the phi29 DNAP translocation step and dNTP binding. We demonstrate that dNTP binds to phi29 DNAP−DNA complexes only after the transition from the pre-translocation state to the post-translocation state; dNTP binding rectifies the translocation but it does not directly drive the translocation. Based on the measured time traces of current amplitude, we developed a method for determining the forward and reverse translocation rates and the dNTP association and dissociation rates, individually at each dNTP concentration and each voltage. The translocation rates, and their response to force, match those determined for phi29 DNAP−DNA binary complexes and are unaffected by dNTP. The dNTP association and dissociation rates do not vary as a function of voltage, indicating that force does not distort the polymerase active site and that dNTP binding does not directly involve a displacement in the translocation direction. This combined experimental and theoretical approach and the results obtained provide a framework for separately evaluating the effects of biological variables on the translocation transitions and their effects on dNTP binding.

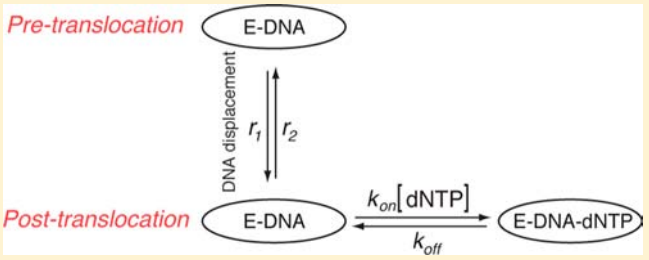

INTRODUCTION

Processive DNA polymerases (DNAPs) are molecular motors that translocate along their DNA substrates in single nucleotide increments during replication. With each step advanced, DNAPs select and bind a 2′-deoxynucleoside triphosphate (dNTP) substrate and catalyze its incorporation into a nascent primer strand. Elucidating the mechanistic relationship between the translocation[1] step and dNTP binding is essential in order to understand how the DNAP motor is driven forward during synthesis. Little is known about the kinetic relationship between the DNAP translocation step and dNTP binding, despite the importance of this relationship to the integration of the translocation step in the nucleotide addition cycle, to the accuracy of the translocation step size, and to the steps in the cycle that ensure correct dNTP selection. Some features of this relationship have been inferred from crystal structures of DNAP−DNA binary complexes and DNAP−DNA−dNTP ternary complexes, which can be considered structural models for the post-translocation and pre-translocation states, respectively.[2−4] In this view, the nascent base pair between the templating base at $n = 0$ and the incoming complementary dNTP in the ternary complex occupies the site that is occupied by the terminal base pair of the duplex in a pre-translocation state complex. Structural studies of both A and B family DNAPs reveal that the binding site for incoming dNTP becomes available following the translocation step, and there is no evidence of a secondary dNTP binding site that might be available in the pre-translocation state.[2−6] However, absence of a secondary binding site does not preclude an influence of dNTP on the translocation step, which could be exerted as a power stroke driven by dNTP binding.[7,8]

The bacteriophage phi29 DNAP is a B-family replicative polymerase that catalyzes highly processive DNA synthesis.[9−11] It accomplishes this without the need for accessory proteins, such as sliding clamps or helicases, because it remains tightly associated with its DNA substrate and it promotes downstream strand displacement during replication.[2,12] The phi29 DNAP is thus an excellent simplified model system for leading strand DNA synthesis catalyzed in more complex replisomes. Processive DNA synthesis catalyzed by individual phi29 DNAP complexes can be monitored at the single molecule level using a nanoscale pore, with single-nucleotide spatial precision and submillisecond temporal resolution.[13−15]

We have shown that phi29 DNAP−DNA complexes fluctuate between the pre-translocation and post-translocation

Received: April 11, 2013
Published: May 24, 2013

   dx.doi.org/10.1021/ja403640b | J. Am. Chem. Soc. 2013, 135, 9149−9155

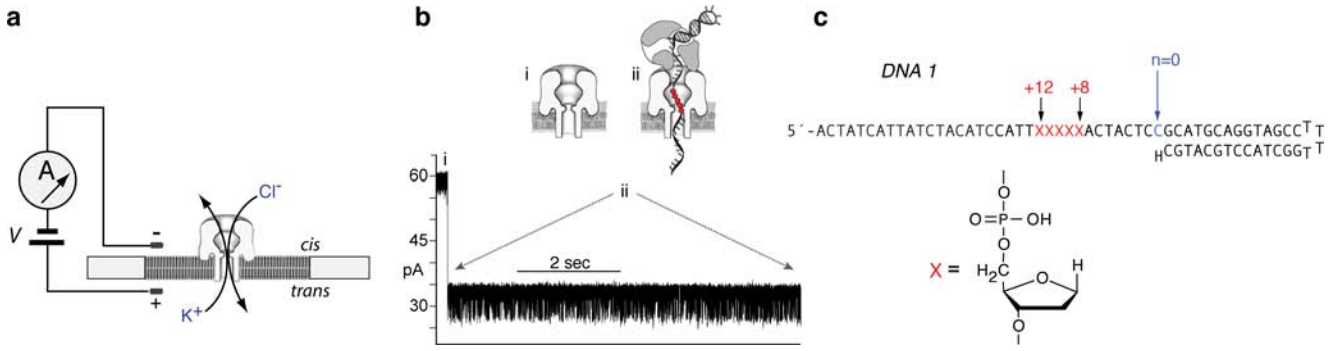

Figure 1. Capture of phi29 DNAP complexes on the α-HL nanopore. In the nanopore device (a), a single α-HL nanopore is inserted in a ~25 μm-diameter lipid bilayer separating two chambers (*cis* and *trans*) that contain buffer solution. A patch clamp amplifier applies voltage across the bilayer and measures ionic current, which is carried through the nanopore by K^+ and Cl^- ions. (b) Representative current trace for a binary complex formed between phi29 DNAP and a DNA substrate (DNA1, in panel c) captured at 180 mV applied potential in buffer containing 10 mM K-Hepes, pH 8.0, 0.3 M KCl, 1 mM EDTA, 1 mM DTT, and 11 mM $MgCl_2$. DNA and phi29 DNAP were added to the nanopore *cis* chamber to final concentrations of 1 and 0.75 μM, respectively. Cartoons above the current trace illustrate the sequence of events, which is described in the text. (c) DNA hairpin substrate (DNA1) featuring a 14-base pair duplex region and a single-stranded template region of 35 nucleotides. The primer strand terminus is a 2′,3′-H CMP residue, and the template strand contains a reporter group of five consecutive abasic (1′,2′-H) residues spanning positions +8 to +12 (indicated as red Xs in the sequence). The structure of an abasic residue is shown below the DNA sequence. In the cartoons in (b), the abasic residues are shown as red circles.

states on the millisecond time scale.[13,16] The fluctuations across the translocation step can be directly observed and quantified when individual complexes are captured atop the α-hemolysin (α-HL) nanopore in an electric field. We have characterized the equilibrium across the translocation step in binary complexes and shown that the presence of complementary dNTP shifts the equilibrium toward the post-translocation state in a concentration-dependent manner.[16] In a study of translocation dynamics, we found that the pre-translocation and post-translocation states are discrete kinetic states and extracted the forward and reverse rates of translocation in phi29 DNAP−DNA binary complexes as functions of applied force and active-site proximal DNA subtrate sequences. The study of translocation dynamics allowed us to characterize features of the free energy landscape of translocation.[13]

In the current study, we have examined quantitatively the kinetic relationship between the translocation step and incoming dNTP binding. We show that dNTP binds to phi29 DNAP−DNA complexes only after they have made the transition from the pre-translocation state to the post-translocation state; dNTP binding rectifies the translocation, but it does not directly drive the translocation. From these findings and previously established results[13,16] we propose a three-state kinetic model for phi29 DNAP−DNA complexes in the presence of dNTP, in which the translocation transition and dNTP binding are sequential. Based on the dynamics of the three-state model and the autocorrelation function of the measured current amplitude,[13,17,18] we have developed a method to extract the forward and reverse rates of the transitions across the translocation step as well as the dNTP association and dissociation rates, as functions of applied force (voltage), which opposes the forward movement of the enzyme. We find that the forward and reverse rates across the translocation step and their dependence on voltage are not influenced by dNTP and are thus an inherent property of phi29 DNAP−DNA binary complexes. The association and dissociation rates for complementary dNTP are unaffected by the applied voltage, indicating that the force does not distort the polymerase active site or perturb any conformational steps associated with complementary dNTP binding.

METHODS

DNA and Enzyme. DNA oligonucleotides were synthesized at Stanford Protein and Nucleic Acid Facility and purified by denaturing PAGE. DNA hairpins were annealed by heating at 90 °C for 4 min followed by snap cooling in ice water. Wild-type phi29 DNAP was obtained from Enzymatics (Beverly, MA).

Nanopore Methods. Nanopore experiments were conducted as described.[16,19−22] Briefly, a single α-HL nanopore is inserted in a ~25 μm-diameter lipid bilayer that separates two chambers containing buffer solution (10 mM K-Hepes, pH 8.0, 0.3 M KCl, and 1 mM EDTA). DTT and $MgCl_2$ were added to the nanopore *cis* chamber to final concentrations of 1 and 11 mM, respectively; DNA and phi29 DNAP were added to the *cis* chamber to final concentrations of 1 and 0.75 μM, respectively; and dGTP was added to the *cis* chamber as indicated in the text and figure legends. Ionic current was measured with an integrating patch clamp amplifier (Axopatch 200B, Molecular Devices) in voltage clamp mode. Data were sampled using an analog-to-digital converter (Digidata 1440A, Molecular Devices) at 100 kHz in whole-cell configuration and filtered at 5 kHz using a low pass Bessel filter.

Extraction of Dwell Time Samples. The dwell time samples in each of the two amplitude states used in the analyses in Figures 2b,c and 4 were extracted using the single-channel detection function in Clampfit 10 (Molecular Devices). This software uses a half amplitude threshold method to assign transitions between two user-defined amplitude levels.[23] Amplitude levels for each of the two states were determined for the single-channel searches from histograms of all sampled amplitude data points. Complexes were captured at 180 mV.

RESULTS AND DISCUSSION

To perform the nanopore experiments, a single α-HL nanopore is inserted into a lipid bilayer separating two chambers (termed *cis* and *trans*) containing buffer solution (Figure 1a). A patch clamp amplifier applies voltage across the bilayer and measures the ionic current that flows through the nanopore, which is carried by K^+ and Cl^- ions in the buffer. Figure 1b shows a representative ionic current trace that results when a complex between phi29 DNAP and a DNA substrate (Figure 1c, DNA1) is captured atop the nanopore at 180 mV applied potential. The ionic current through the pore (Figure 1b, i) drops rapidly when a complex is captured (Figure 1b, ii). The polymerase is too large to enter the nanopore, and it thus holds the duplex

dx.doi.org/10.1021/ja403640b | J. Am. Chem. Soc. 2013, 135, 9149−9155

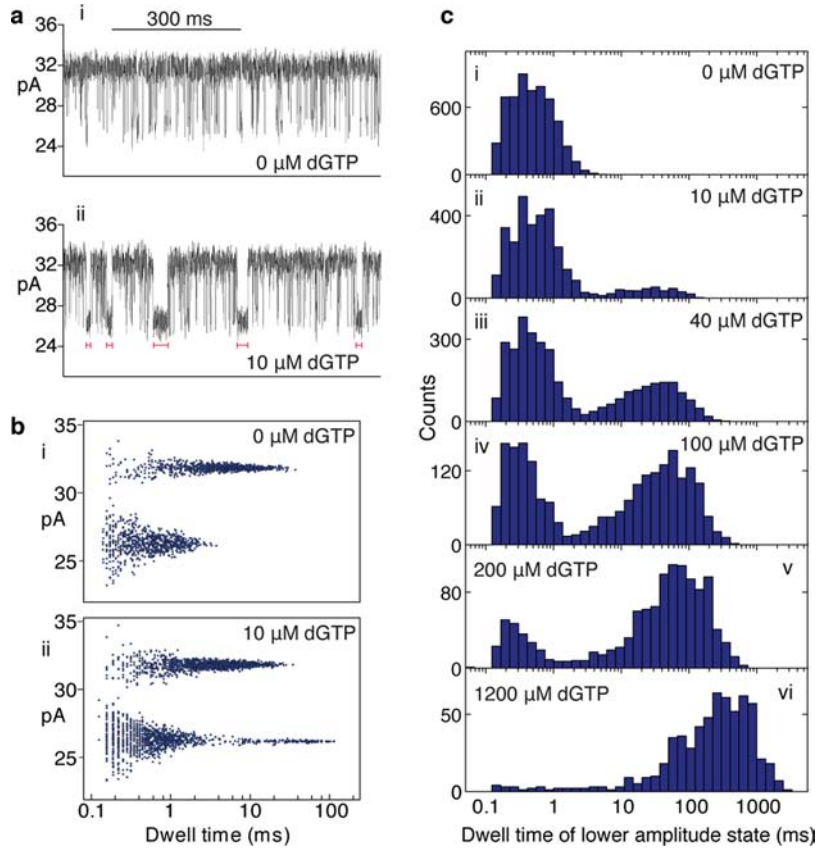

Figure 2. Complementary dNTP binding to phi29 DNAP complexes. (a) Ionic current traces for phi29 DNAP−DNA1 complexes, captured at 180 mV in the presence of 0 μM (i) or 10 μM (ii) dGTP. In the presence of dGTP, some of the transitions to the lower amplitude, post-translocation state have dwell times that are significantly longer than those typically observed in the absence of dGTP (indicated by red lines under the trace in ii). (b) Plots of log dwell time vs amplitude for dwell time samples extracted from complexes captured at 180 mV in the presence of 0 μM (i) or 10 μM (ii) dGTP. In the absence of dNTP (i) there are two clusters that are well separated in amplitude: the pre-translocation state dwell time samples centered at ∼32 pA, and a cluster of post-translocation state samples centered at ∼26 pA. Upon addition of dGTP (ii) a third cluster, with longer dwell times, emerges at the post-translocation state amplitude. (c) Histograms of log dwell time samples of the post-translocation, lower amplitude state centered at ∼26 pA, extracted from ionic current traces for complexes captured at the indicated dGTP concentrations.

portion of the DNA substrate atop the pore. The DNA template strand of the captured complex is suspended through the pore lumen, which is just wide enough to accommodate a single strand of DNA.

Captured phi29 DNAP−DNA complexes reside atop the nanopore for several seconds (Figure 1b, ii), during which the measured ionic current fluctuates on the millisecond time scale between two amplitude levels. These fluctuations are due to movement of the DNA substrate relative to the enzyme and the nanopore; the distance of this displacement is approximately one nucleotide.[16] Detection of the DNA displacement is achieved by the use of a reporter group comprising five consecutive abasic (1′, 2′-H) residues in the template strand (Figure 1c). The fluctuations between the two amplitude levels are detected when the reporter group is displaced in the nanopore lumen.[16] In the upper amplitude state, the primer−template junction of the DNA substrate is bound in the polymerase active site, in the pre-translocation state. At 180 mV, the pre-translocation state amplitude is centered at ∼32 pA. In the lower amplitude state, the primer−template junction of the DNA substrate resides in the polymerase active site, in the post-translocation state.[16] The post-translocation state amplitude is centered at ∼26 pA at 180 mV. The amplitude fluctuations continue until complexes dissociate or are ejected, after which another complex can be captured.

Complementary dNTP Binding to phi29 DNAP Complexes. The primer strand of DNA1 bears a 2′-H, 3′-H terminus (Figure 1c) rather than the 2′-H, 3′-OH terminus of the natural substrate; DNA1 therefore supports the formation of phi29 DNAP−DNA−dNTP ternary complexes but not the chemical step of phosphodiester bond formation. Binding of dGTP (complementary to the template dCMP residue at n = 0) to phi29 DNAP−DNA1 complexes stabilizes the post-translocation state.[16] The effect of dGTP can be directly observed in the current traces (Figure 2a). In the absence of dNTP, complexes fluctuate rapidly between the two states (Figure 2a, i); the addition of dGTP (10 μM; Figure 2a, ii) causes the dwell time of the lower amplitude, post-translocation state to increase, due to the emergence of a subpopulation with longer dwell times.

We used a half amplitude threshold method[23] to extract dwell time samples from ionic current traces for phi29 DNAP−DNA1 complexes, captured at 180 mV, in the absence or presence of dGTP. A plot of log dwell time vs amplitude for dwell time samples extracted from complexes captured at 0 μM dGTP (Figure 2b, i) shows two clusters that are well-separated in amplitude: the pre-translocation state dwell time samples centered at ∼32 pA, and a cluster of post-translocation state samples centered at ∼26 pA. Upon addition of dGTP (10 μM; Figure 2b, ii), a new cluster, with longer dwell times, emerges at

dx.doi.org/10.1021/ja403640b | J. Am. Chem. Soc. 2013, 135, 9149−9155

the post-translocation state amplitude of ~26 pA. Histograms of log dwell time distribution for the dwell time samples at the post-translocation state amplitude, extracted from ionic current traces for complexes captured at different dGTP concentrations, are shown in Figure 2c. Binary complexes (0 μM dGTP) have a distribution centered at ~0.4 ms (Figure 2c, i). When dGTP is titrated into the chamber, a second cluster emerges with dwell time centered at ~30 ms (Figure 2c, ii). As the dGTP concentration is increased, the counts in the longer dwell time cluster, attributable to post-translocation state phi29 DNAP–DNA–dGTP ternary complexes, increase. As the dGTP concentration increases above ~10 μM dGTP, this post-translocation state ternary complex cluster also shifts toward longer dwell times (Figure 2c, iii–vi).

The Kinetic Relationship between Translocation and dNTP Binding. In studying the equilibrium properties of the phi29 DNAP translocation step and the effects of complementary dNTP binding on the equilibrium across this step, we used a four-state model that made no assumptions about which transitions between the four states were permitted or about which of the two translocation states were competent to bind dNTP (Figure 3a). We found that while complementary dNTP binds with high affinity to complexes in the post-translocation state (K_d ~1.4 μM), complexes in the pre-translocation state have negligible affinity for dNTP,[16] ruling out the existence of a stable dNTP-bound pre-translocation state (Figure 3a, blue dashed oval). There are two kinetic schemes that are consistent with this behavior: In one scheme, dNTP can facilitate the transition from the pre-translocation to the post-translocation state and can bind to complexes in the post-translocation state (Figure 3b). In the second scheme, dNTP can bind to complexes only once they have reached the post-translocation state; dNTP binding rectifies the complex in the post-translocation state, but it does not directly drive the translocation (Figure 3c).

To distinguish between the models in Figure 3b,c, we used dwell time samples extracted from current traces of phi29 DNAP–DNA1 complexes, captured at 180 mV in the absence or presence of dGTP. Each dwell time sample in the upper amplitude, pre-translocation state (Figure 4a, ΔT_{pre}) is followed by a dwell time sample in the lower amplitude, post-translocation state (Figure 4a, ΔT_{post}). In the three-state model shown in Figure 3b, there are two transition pathways from the pre-translocation state to the post-translocation state. The two transition rates are r_1 and r_3[dGTP]. The mean dwell time of the pre-translocation state satisfies:

$$1/\langle \Delta T_{pre} \rangle = r_1 + r_3[\mathrm{dGTP}]$$

Subtracting $1/\langle \Delta T_{pre} \rangle|_{[\mathrm{dGTP}]=0} = r_1$ from the equation above and dividing by [dGTP], we can express r_3, the first-order rate constant of the dGTP-binding driven translocation, in terms of measured mean dwell times:

$$r_3 = (1/\langle \Delta T_{pre} \rangle - 1/\langle \Delta T_{pre} \rangle_{|[\mathrm{dGTP}]=0})/[\mathrm{dGTP}]$$

Both $\langle \Delta T_{pre} \rangle$ and $\langle \Delta T_{pre} \rangle|_{[\mathrm{dGTP}]=0}$ have statistical uncertainty caused by the finite sample size. Since $\langle \Delta T_{pre} \rangle$ and $\langle \Delta T_{pre} \rangle|_{[\mathrm{dGTP}]=0}$ are measured in separate experiments, they are also affected by experimental uncertainty. We estimated the values of r_3 from data collected at 200 and 1200 μM dGTP (the two highest concentrations tested), because at low [dGTP] the uncertainties are magnified and because if a [dNTP]-dependent transition exists it would be more prominent at the higher concentrations. The estimated values of r_3 are

$$[\mathrm{dGTP}] = 200\mu\mathrm{M}: \quad r_3 = (-0.040 \pm 0.037)\mu\mathrm{M}^{-1}\mathrm{sec}^{-1}$$

$$[\mathrm{dGTP}] = 1200\mu\mathrm{M}: \quad r_3 = (0.053 \pm 0.011)\mu\mathrm{M}^{-1}\mathrm{sec}^{-1}$$

Taking into consideration the statistical uncertainties (the standard errors given above) and the experimental uncertainties

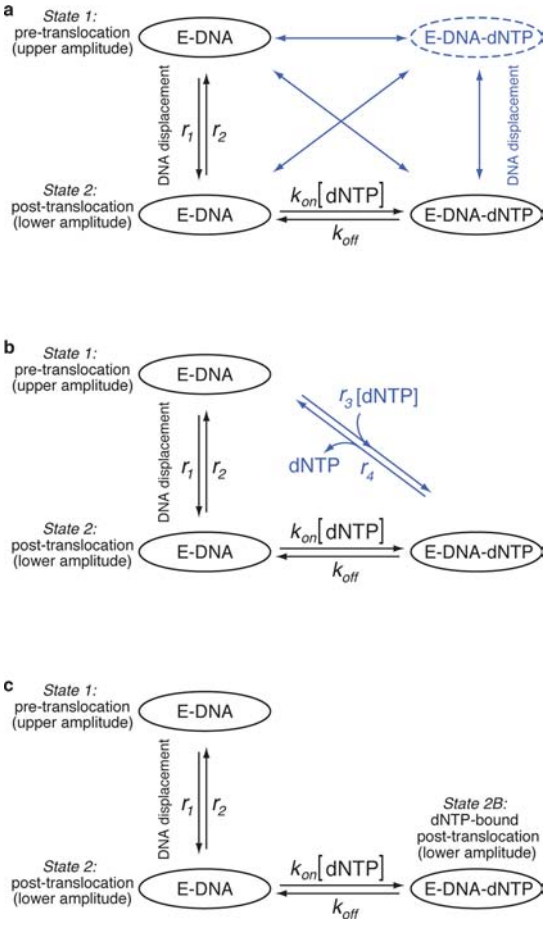

Figure 3. Potential models for the kinetic relationship between translocation and dNTP binding. Phi29 DNAP–DNA binary complexes fluctuate between the pre-translocation and post-translocation states with the forward rate r_1 and the reverse rate r_2. (a) The four-state model used for studying the equilibrium properties of translocation state transitions in phi29 DNAP–DNA complexes. This model includes no assumptions about the transitions that are permitted between the four states or about in which of the two translocation states complexes can bind dNTP. The existence of the dNTP-bound pre-translocation state (dashed blue oval) was ruled out by the results of the equilibrium study.[16] (b) A three-state model in which dNTP can influence the transition from the pre-translocation to the post-translocation state (r_3[dNTP]) and can bind to complexes in the post-translocation state (k_{on}[dNTP]). Dissociation of dNTP can occur prior to (k_{off}) and concurrent with (r_4) the transition from the post-translocation to the pre-translocation state. In the current study, we rule out this model by showing $r_3 \approx 0$ and $r_4 \approx 0$ (Figure 4). (c) A three-state model in which translocation and dNTP binding are sequential: dNTP can bind to complexes only after the transition from the pre-translocation to the post-translocation state (k_{on}[dNTP]); the transition from the post-translocation to the pre-translocation state cannot occur before the dissociation of dNTP (k_{off}). This is the model used in the current study to determine transition rates from measured time traces of current amplitude.

dx.doi.org/10.1021/ja403640b | J. Am. Chem. Soc. 2013, 135, 9149–9155

(as manifested in that the estimated value of r_3 is negative at [dGTP] = 200 μM), we conclude $r_3 < 0.1\ \mu M^{-1}sec^{-1}$. Thus, r_3 is negligible, indicating that the transition from the pre-translocation to the post-translocation is not driven or initiated by dNTP; the translocation transition must precede dNTP binding in phi29 DNAP–DNA complexes.

The principle of microscopic reversibility dictates that if the pathway in which dNTP influences the transition from the pre-translocation to post-translocation state (r_3; Figure 3b) does not exist, then dNTP dissociation from the post-translocation state ternary complex must precede the transition from the post-translocation to pre-translocation state. The rate of direct transition from the dNTP-bound post-translocation state to the pre-translocation state (r_4; Figure 3b) can also be estimated from experimental data (Figure 4b). Since dNTP stabilizes the post-translocation state in a concentration-dependent manner without saturation,[16] and r_4 is independent of [dNTP], at [dGTP] = infinity, $1/\langle \Delta T_{post} \rangle = r_4$. As we cannot directly measure data at [dGTP] = ∞, we use the theoretical expression (at high[dGTP]):

$$1/\langle \Delta T_{post} \rangle \approx \alpha/[\mathrm{dGTP}] + r_4$$

to extrapolate from data points at high [dGTP] mathematically to [dGTP] = ∞ (see Supporting Information for derivation). Figure 4b shows the measured data points of 1/[dGTP] vs $1/\langle \Delta T_{post} \rangle$ with error bars. Carrying out linear extrapolation to 1/[dGTP] = 0, we estimate the direct transition rate as $r_4 = 0.04 \pm 0.3\ s^{-1}$. Since the estimated value is much smaller than the error range, we conclude that within the given error range we have $r_4 = 0$; the direct transition from the dNTP-bound post-translocation state to the pre-translocation state has zero rate within the error range. Thus, dNTP that is bound to complexes in the post-translocation state must be released prior to the transition to the pre-translocation state.

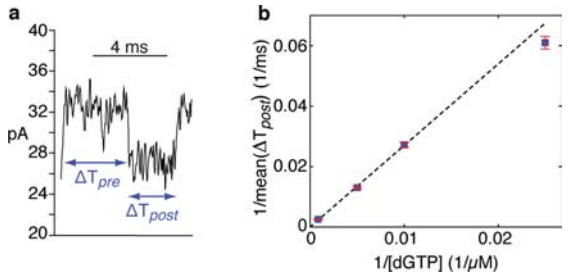

Figure 4. The kinetic relationship between translocation and dNTP binding. (a) Segment of current trace from a phi29 DNAP–DNA1 complex captured at 180 mV, showing a pair of dwell time samples. The ionic current fluctuates discretely between the two amplitude states; thus each dwell time sample in the upper amplitude pre-translocation state (ΔT_{pre}) is followed by a sample in the post-translocation state (ΔT_{post}). (b) In the plot of 1/[dGTP] vs $1/\langle \Delta T_{post} \rangle$, the error bars represent standard errors. The standard error of $1/\langle \Delta T_{post} \rangle$ is given by $SE(1/\langle \Delta T_{post} \rangle) = SE(\langle \Delta T_{post} \rangle)/\langle \Delta T_{post} \rangle^2$, where the standard error of $/\langle \Delta T_{post} \rangle$ is calculated from independent samples of ΔT_{post}. Theoretically, we expect that $1/\langle \Delta T_{post} \rangle \approx \alpha/[\mathrm{dGTP}] + r_4$ at high [dGTP], where r_4 is the rate of direct transition from the dNTP-bound post-translocation to the pre-translocation state (Figure 3B). Fitting a straight line to data of 3 highest concentrations, [dGTP] = 100, 200, and 1200 μM, we obtain $r_4 = (0.04 \pm 0.3) \times 10^{-3}(ms)^{-1} = (0.04 \pm 0.3)\ sec^{-1}$. Thus, we conclude that $r_4 = 0$ within the given error range.

These analyses support the conclusions that: (i) dNTP can bind to phi29 DNAP–DNA complexes only after the transition from the pre-translocation to the post-translocation state; (ii) upon dNTP binding, the complex is locked in the post-transocation state; (iii) transition back to the pre-translocation state cannot occur before the dissociation of dNTP; and (iv) the dNTP binding process is not coupled or correlated with the transition process between the two translocation states. In particular, the dNTP binding process does not directly drive the transition from the pre-translocation to post-translocation state. We therefore adopt the three-state kinetic model shown in Figure 3c, in which the transition to the post-translocation state and the dNTP binding are sequential.

A Three-State Kinetic Model for Translocation and dNTP Binding. In the model (Figure 3c), the phi29 DNAP–DNA complex has three states: (i) pre-translocation state (upper amplitude), state 1; (ii) post-translocation state (lower amplitude), state 2; and (iii) post-translocation state with dGTP bound (lower amplitude), state 2B.

The two post-translocation states yield the same ionic current amplitude. The three states are connected by four transition rates: r_1, r_2, k_{on}[dGTP], and k_{off}. Below we briefly describe a method for estimating the four transition rates from data at individual values of voltage and [dGTP]. All mathematical derivations are given in the Supporting Information. I_1 is the mean amplitude of the pre-translocation state; I_2 is the mean amplitude of post-translocation state; and $X(t)$ is measured time trace of amplitude.

We consider the scaled amplitude:

$$Y(t) = \frac{2}{(I_1 - I_2)}\left(X(t) - \frac{I_1 + I_2}{2}\right)$$

The mean of $Y(t)$, denoted by $E[Y]$, is calculated directly from the data. The autocorrelation $R(t) \equiv E[Y(t_0)Y(t_0+t)]$ has the expressions (see Supporting Information):

$$R(t) = (E[Y])^2 + (1 - (E[Y])^2)[c_1\exp(-\lambda_1 t) + (1 - c_1)\exp(-\lambda_2 t)]$$

$R(t)$ is calculated directly from the data. Quantities c_1, λ_1, and λ_2 are obtained by fitting the measured $R(t)$ to the given function form. Measured $E[Y]$, c_1, λ_1, and λ_2 are related to the four transition rates (see Supporting Information) as:

$$\frac{\frac{r_2}{r_1} - \left(1 + \frac{[\mathrm{dGTP}]}{K_d}\right)}{1 + \frac{[\mathrm{dGTP}]}{K_d} + \frac{r_2}{r_1}} = E[Y]$$

$$\frac{4r_2}{1 + \frac{[\mathrm{dGTP}]}{K_d} + \frac{r_2}{r_1}} = (1 - (E[Y])^2)[c_1\lambda_1 + (1 - c_1)\lambda_2]$$

$$r_1 k_{off}\left(\frac{r_2}{r_1} + \frac{[\mathrm{dGTP}]}{K_d} + 1\right) = \lambda_1 \cdot \lambda_2$$

$$(r_1 + r_2) + (k_{on}[\mathrm{dGTP}] + k_{off}) = \lambda_1 + \lambda_2$$

In the four equations above, all quantities on the right-hand side are calculated from data. The four transition rates are solved from these four equations. Thus, we can estimate a set of four transition rates from each measured time trace of ionic current amplitude. At each individual voltage and [dGTP], we have measured time traces from 20 to 60 individual captured

dx.doi.org/10.1021/ja403640b | J. Am. Chem. Soc. 2013, 135, 9149–9155

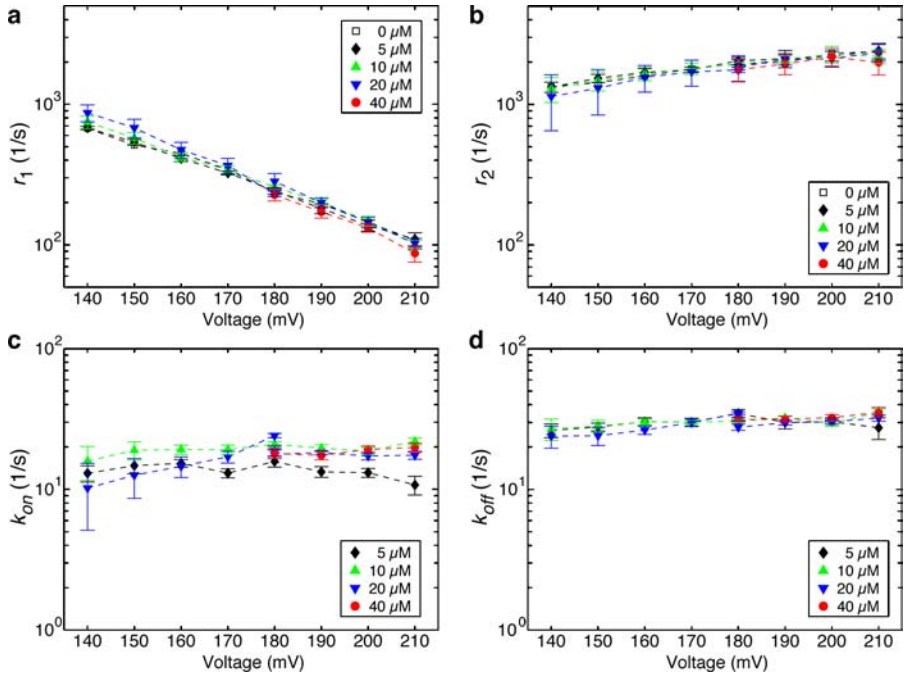

Figure 5. Translocation rates and dNTP association and dissociation rates determined from the three-state model. Plots of (a) $\log(r_1)$ vs voltage and (b) $\log(r_2)$ vs voltage for phi29 DNAP–DNA1 complexes captured in the presence of 0, 5, 10, 20, or 40 μM dGTP. Plots of (c) k_{on} vs voltage and (d) k_{off} vs voltage for complexes captured in the presence of 5, 10, 20, or 40 μM dGTP. Rates were extracted from ionic current traces using the autocorrelation function and the three-state model in Figure 3c. The data for $\log(r_1)$ vs voltage and $\log(r_2)$ vs voltage for phi29 DNAP–DNA1 binary complexes (0 μM dGTP) are from ref 13. Because k_{on} is calculated by dividing the apparent rate by the concentration of dGTP added to the experiments, the variability in the values for this rate may be attributable to small differences in the actual dGTP concentration between experiments due to pipeting inaccuracies. Errors bars indicate the standard error. Numerical values for the rates and standard errors are given in Table S1.

complexes. From the multiple estimated sets of parameter values, we use the mean as a more accurate estimate and use the standard error as the error bar.

Translocation Rates and dNTP Binding Rates in phi29 DNAP–DNA Complexes. Using the method described above, we determined the forward (r_1) and reverse (r_2) rates across the translocation step and the association (k_{on}[dNTP]) and dissociation (k_{off}) rates of dNTP binding, for phi29 DNAP complexes captured across a range of applied voltages and at several dGTP concentrations. We extracted the rates from the data files collected under each condition separately. The effects of applied force and dGTP concentration on the four transition rates are plotted in Figure 5.

We have shown that for phi29 DNAP–DNA binary complexes, $\log(r_1)$ and $\log(r_2)$ vary as a linear function of the applied voltage.[13] Because dNTP does not influence the transition from the pre-translocation to post-translocation state and must dissociate prior to the transition from the post-translocation to pre-translocation state (Figure 4), the values of r_1 and r_2 (at each voltage) derived by applying the three-state model to data collected in the presence of dGTP are predicted to be same as the values of r_1 and r_2 previously determined for binary complexes (0 μM dGTP) using a robust two-state model.[13] Plots of $\log(r_1)$ vs voltage (Figure 5a) and $\log(r_2)$ vs voltage (Figure 5b) for complexes captured in the presence of 0, 5, 10, 20, or 40 μM dGTP verify this prediction; the vertical intercepts and the slopes of $\log(r_1)$ vs voltage and $\log(r_2)$ vs voltage are unaffected by dGTP concentration, indicating that dGTP does not influence the rates at a given voltage or the dependence of the rates on voltage. The rates across the translocation step are an inherent property of phi29 DNAP–DNA binary complexes and are independent of the presence or absence of dNTP.

Plots of k_{on} vs voltage (Figure 5c) and k_{off} vs voltage (Figure 5d) show that these binding rates do not vary as a function of [dGTP] or applied voltage (across the range of voltages tested). The absence of an effect of voltage on the dNTP association and dissociation rates is consistent with our prior conclusion that the K_d for dNTP binding is independent of the voltage.[16] We can conclude two things from the finding that opposing force in the translocation direction does not affect the dNTP association or dissociation rates: (i) dNTP binding (or dissociation) does not directly involve a displacement in the translocation direction. The effect of the applied force on the free energy difference between the two states is proportional to the displacement along the direction of the force. If the free energy difference is varied, at least one transition rate must be affected; (ii) the opposing force in the translocation direction does not distort the polymerase active site or perturb any conformational steps that may be associated with complementary dNTP binding. In addition to changing the free energy difference, force can influence the dynamic transition rates by changing the free energy barrier between the two states. The plots of k_{on} and k_{off} vs voltage show that the free energy landscape associated with dNTP binding is unaffected by opposing force in the translocation direction. Since neither k_{on} nor k_{off} displays a systematic trend with the applied voltage or [dGTP], by treating all data points in each panel as independent samples, we calculate the mean and standard error for each of these two rates as k_{on} = 17.46 ± 0.60 $\mu M^{-1}sec^{-1}$ and k_{off} = 30.18 ± 0.54 s^{-1}.

The three-state model and the values determined for the four transition rates provide a rationale for the increase in dwell time

dx.doi.org/10.1021/ja403640b | J. Am. Chem. Soc. 2013, 135, 9149–9155

of the dNTP-dependent post-translocation state cluster observed in dwell time histograms as [dGTP] is increased (Figure 2c). The 3′-H terminus of DNA1 prevents phosphodiester bond formation, and thus bound dGTP dissociates from phi29 DNAP complexes, at the rate k_{off}. After dGTP dissociation, the complex has two possible fates; it can transition to the pre-translocation state at rate r_2, or another molecule of dGTP can bind with the rate k_{on}[dGTP]. At a given voltage, as the concentration of dGTP is increased, the rate of association increases, while r_2 does not change; therefore the probability that another dGTP molecule will bind before the complex can transition to the pre-translocation state increases. There is a kinetic competition between k_{on} and r_2 that leads to an continual increase in post-translocation state dwell time as [dGTP] is increased (Figure 2c) due to iterative binding of dGTP to complexes in the post-translocation state.

CONCLUSION

The results of this study, taken together with our prior studies on the equilibrium properties of the translocation step[16] and the dynamics of the translocation fluctuations in phi29 DNAP binary complexes,[13] yield an integrated model for the kinetic mechanism of translocation and dNTP binding for phi29 DNAP. The pre-translocation and the post-translocation states are two metastable states, separated by an energy barrier. Fluctuations between the two states are driven by Brownian thermal motion, and complexes are rectified in the post-translocation state by dNTP binding. There is no direct transition between the pre-translocation state to the dNTP bound post-translocation state: dNTP can bind only when the complex is in the post-translocation state, and dNTP binding does not directly drive any movement along the translocation direction. Conversely, dNTP dissociation does not directly involve any translocation displacement, and it must precede the transition back to the pre-translocation state. The rates of transitions between the pre-translocation and post-translocation states, the response of those rates to applied force and the energy landscape of the spatial displacement across the translocation step are inherent properties of phi29 DNAP–DNA binary complexes and are not influenced by the presence of dNTP. Furthermore, the rates of dNTP binding and dissociation are not affected by the opposing force in the translocation direction, confirming that neither dNTP binding nor dissociation is directly accompanied by any displacement in the translocation direction.

The current study yields the capability to quantify the effects of duplex mismatches, rNMPs in the duplex or in the template strand, or polymerase mutations on the translocation state transitions separately from their effects on dNTP binding to complexes in the post-translocation state. The effects of alterations in the base or sugar moieties of nucleotide substrates on binding to the post-translocation state can be determined. In addition, this study provides a quantitative kinetic framework in which to evaluate processive DNA synthesis catalyzed by phi29 DNAP at the single molecule level as a function of controlled opposing force.

ASSOCIATED CONTENT

Supporting Information

Text (mathematical derivations) and Table S1 (translocation and dNTP binding rates at each voltage and each dNTP concentration). This material is available free of charge via the Internet at http://pubs.acs.org.

AUTHOR INFORMATION

Corresponding Author

krlieberman@gmail.com; hongwang@soe.ucsc.edu

Notes

The authors declare no competing financial interest.

ACKNOWLEDGMENTS

We are grateful to Robin Abu-Shumays for helpful discussions. This work was supported by NIH grant 1R01GM087484 from NIGMS (to K.R.L. and M.A.) and by NSF grant DMS-0719361 (to H.W.).

REFERENCES

(1) Throughout this study, we use the term translocation to refer to the movement of phi29 DNAP with respect to its DNA substrate. We do not use the term translocation to refer to the passage of DNA from one side of the nanopore chamber to the other.

(2) Berman, A. J.; Kamtekar, S.; Goodman, J. L.; Lázaro, J. E. M.; de Vega, M.; Blanco, L.; Salas, M.; Steitz, T. A. *EMBO J.* **2007**, *26*, 3494–3505.

(3) Golosov, A. A.; Warren, J. J.; Beese, L. S.; Karplus, M. *Structure* **2010**, *18*, 83–93.

(4) Johnson, S. J.; Taylor, J. S.; Beese, L. S. *Proc. Natl. Acad. Sci. U.S.A.* **2003**, *100*, 3895–3900.

(5) Doublié, S.; Tabor, S.; Long, A. M.; Richardson, C. C.; Ellenberger, T. *Nature* **1998**, *391*, 251–258.

(6) Franklin, M. C.; Wang, J.; Steitz, T. A. *Cell* **2001**, *105*, 657–667.

(7) Wang, H.; Oster, G. *Appl. Phys. A: Mater. Sci. Process.* **2002**, *75*, 315–323.

(8) Oster, G.; Wang, H. *Trends Cell Biol.* **2003**, *13*, 114–121.

(9) Blanco, L.; Bernad, A.; Lázaro, J. M.; Mart i n, G.; Garmendia, C.; Salas, M. *J. Biol. Chem.* **1989**, *264*, 8935–8940.

(10) Blanco, L.; Salas, M. *J. Biol. Chem.* **1996**, *271*, 8509–8512.

(11) Salas, M.; Blanco, L.; Lázaro, J. E. M.; de Vega, M. *IUBMB Life* **2008**, *60*, 82–85.

(12) Morin, J. A.; Cao, F. J.; Lázaro, J. M.; Arias-Gonzalez, J. R.; Valpuesta, J. M.; Carrascosa, J. L.; Salas, M.; Ibarra, B. *Proc. Natl. Acad. Sci. U.S.A.* **2012**, *109*, 8115–8120.

(13) Lieberman, K. R.; Dahl, J. M.; Mai, A. H.; Akeson, M.; Wang, H. *J. Am. Chem. Soc.* **2012**, *134*, 18816–18823.

(14) Cherf, G. M.; Lieberman, K. R.; Rashid, H.; Lam, C. E.; Karplus, K.; Akeson, M. *Nat. Biotechnol.* **2012**, *30*, 344–348.

(15) Manrao, E. A.; Derrington, I. M.; Laszlo, A. H.; Langford, K. W.; Hopper, M. K.; Gillgren, N.; Pavlenok, M.; Niederweis, M.; Gundlach, J. H. *Nat. Biotechnol.* **2012**, *30*, 349–353.

(16) Dahl, J. M.; Mai, A. H.; Cherf, G. M.; Jetha, N. N.; Garalde, D. R.; Marziali, A.; Akeson, M.; Wang, H.; Lieberman, K. R. *J. Biol. Chem.* **2012**, *287*, 13407–13421.

(17) Bezrukov, S. M.; Kasianowicz, J. J. *Phys. Rev. Lett.* **1993**, *70*, 2352–2355.

(18) Kogan, S. *Electronic Noise and Fluctuations in Solids*; Cambridge University Press: New York, 1996.

(19) Lieberman, K. R.; Cherf, G. M.; Doody, M. J.; Olasagasti, F.; Kolodji, Y.; Akeson, M. *J. Am. Chem. Soc.* **2010**, *132*, 17961–17972.

(20) Benner, S.; Chen, R. J. A.; Wilson, N. A.; Abu-Shumays, R.; Hurt, N.; Lieberman, K. R.; Deamer, D. W.; Dunbar, W. B.; Akeson, M. *Nat. Nanotechnol.* **2007**, *2*, 718–724.

(21) Akeson, M.; Branton, D.; Kasianowicz, J. J.; Brandin, E.; Deamer, D. W. *Biophys. J.* **1999**, *77*, 3227–3233.

(22) Garalde, D. R.; Simon, C. A.; Dahl, J. M.; Wang, H.; Akeson, M.; Lieberman, K. R. *J. Biol. Chem.* **2011**, *286*, 14480–14492.

(23) Colquhoun, D.; Sigworth, F. J. In *Single-channel recording*; Sakmann, B., Neher, E., Eds.; Plenum Press: New York, 1995; pp 483–587.